Pacific Ocean precursors anticipate strong 2014/2015 El Niño

Di Lorenzo[1*] E., K.M. Cobb[1], Axel Timmerman[2], Matthew Newman[3], Niklas Schneider[0], Bruce Anderson[4], Matthew J. Widlansky[2], Howard Freeland[5]

[1] *School of Earth and Atmospheric Sciences, Georgia Institute of Technology, GA, USA*

[2] *International Pacific Research Center, University of Hawaii at Manoa, HI, USA*

[3] *CIRES, University of Colorado and NOAA/ESRL/PSD, Boulder, CO 80305, USA.*

[4] *Department of Earth and the Environment, Boston University, Boston, MA, 02215, USA*

[5] *Institute of Ocean Sciences, DFO, Sidney, BC, V8L 4B2, Canada*

Submitted to *Nature Geoscience*

[*]Corresponding Author:
Emanuele Di Lorenzo
School of Earth and Atmospheric Sciences
Georgia Institute of Technology
311 Ferst Drive, Atlanta, GA 30332
Email: edl@gatech.edu

Abstract

The El Niño-Southern Oscillation (ENSO) phenomenon impacts the global climate system, shifting weather pattern[1], affecting terrestrial and marine ecosystem[2], and sea level distributions[3]. While some studies link the interannual frequency of El Niño events to oscillatory ocean dynamics[4], others highlight the importance of random tropical[5,6] and extratropical[7-9] atmospheric perturbations in triggering El Niño events. In winter/spring 2013/2014 these atmospheric triggers, also known as "precursors", were very active, leading to strong westerly wind burst activity and subsurface warming (~6 °C) in the equatorial Pacific and record-breaking sea surface temperature anomalies in the North Pacific (~3 °C). The similarity of these conditions to the one observed in the winter/spring prior to the large 1997/98 El Niño (>3 °C), has raised concerns that a strong El Niño event is developing for the winter of 2014/2015[10]. Here, we develop a physically-based statistical ENSO model that combines both extratropical and tropical precursor dynamics. This model exhibits significant hindcast skill in identifying the 1972/73, 1982/83, and 1997/98 El Niños as strong events (>2 °C), and relates them to years when both tropical and extra-tropical triggers were active and strong in the preceding winter/early spring. Furthermore, stochastic simulations of the model are in agreement with observational statistics of El Niño return times, thus supporting the random event paradigm[5] and challenging the idea that memory is retained from one event to the next. Applied to the current situation with several precursors active, the model predicts the development of a strong 2014/2015 El Niño event.

Previous studies document how tropical stochastic atmospheric forcing associated with equatorial westerly wind bursts (WWB) and the Madden-Julian oscillation can generate perturbations in the coupled ocean-atmosphere system of the tropical Pacific that generate El Niño events with lead times of about half-a-year or longer[6,11-16]. Additionally, more recent studies show that extratropical stochastic atmospheric variability in the North Pacific can also trigger tropical sea surface temperature anomalies[8,9,17-19]. The action of stochastic forcing for a stable ENSO system is more effective when the equatorial thermocline is charged[4] – for example when the west Pacific thermocline is deeper than usual.

The spatial structure of the tropical and extra-tropical precursors of El Niño can be seen by regressing ocean temperatures and zonal surface winds over the period of Jan-Feb-Mar-Apr (JFMA) on the December Niño3 index, which represents the mature phase of El Niño (Figure 1). Along the equator the tropical precursor is characterized by positive anomalies in the statistics of westerly wind bursts (Figure 1a, orange arrow) and positive subsurface temperature anomalies in the thermocline[20]. In the North Pacific, the precursor pattern exhibits a horseshoe shape in SST anomalies (SSTa) around the latitudes of the Hawaiian Islands[7,18,20]. Both the tropical and extra-tropical precursor patterns were observed in the JFMA prior to the strong 1997/98 and 1982/83 El Niño events (Figure 1c–f). A visual comparison of these precursor patterns with the anomalies observed during 2014 reveals an intriguing correspondence (Figure 1g and h). In March and April 2014 the tropical Pacific was

77 characterized by sustained westerly winds and anomalous subsurface warming
78 (~6°C). In the North Pacific a large body of warm water with record-breaking
79 temperatures of 3°C (ref. 21) formed a portion of the North Pacific SSTa
80 precursor pattern. While the temperature and wind anomalies in JFMA of 2014
81 closely resembled the El Niño precursors of the strong 1997/98 event, a more
82 quantitative approach is needed to determine how and if this alignment of
83 preconditioning factors translates into moderate or strong El Niño conditions.

84 To develop a simple statistical model of El Niño that takes into account the
85 tropical and extra-tropical precursors, we need to define some physically-based
86 indices of these two stochastic triggers. To start, we note that the North Pacific
87 SSTa precursor (Figure 1b), first isolated by (ref. 7) and commonly referred to
88 as the 'Meridional Mode' (refs. 17,22), is excited by stochastic atmospheric
89 variability in the extra-tropical trade winds[8]. Indeed, the spatial structure of the
90 North Pacific meridional mode emerges statistically as the second dominant
91 mode of co-variability between Pacific SSTa and sea level pressure anomalies
92 (SLPa) (Figure 2) (see also methods). This co-variability mode is characterized
93 by an atmospheric spatial pattern (Figure 2a, SLPa), an ocean pattern (Figure 2b
94 SSTa) and a Principal Component (PC) timeseries. Further, the PC timeseries of
95 this 2nd mode (Figure 2c, PC_{PREC} blue line) exhibits a consistent relationship
96 with the 1st dominant mode, which tracks the El Niño Southern Oscillation
97 (ENSO). Specifically the meridional mode leads the ENSO mode by ~12 months
98 with significant correlations R=0.62. The SSTa signature of the meridional
99 mode shows the typical horseshoe-warming pattern of the North Pacific

100 precursors (see Figure 1a), while the SLPa structure shows a strong pole of
101 negative anomalies over the Hawai'i region.

102 Studies of the meridional mode have shown that stochastic variability in
103 the Hawaiian SLPa pole excites thermodynamic coupling between the ocean and
104 atmosphere (e.g. via the wind-evaporation-SST feedback[23]) generating SSTa in
105 the tropical Pacific that energize the ENSO mode[19]. Other studies have linked
106 the Hawaiian SLPa pole to the generation of subsurface waves[24] and the
107 charging of equatorial heat content[9,25], both of which can also initiate ENSO
108 responses. Whereas the relative roles of these extra-tropical precursor dynamics
109 need to be further explored, it is clear that SLPa variability in the Hawaiian
110 region [10°N-20°N; 160°W-140°W] (Figure 2a, blue rectangle) can be used to
111 develop a simple index of the North Pacific precursor dynamics (SLPHI, see
112 methods) (Figure 3a).

113 An index for the tropical Pacific stochastic precursor can be defined using
114 the zonal wind anomalies and WWB statistics (WWBI), which are typically
115 observed in the western equatorial Pacific 6-9 months prior to the development
116 of a mature El Niño event. We construct an index of WWB activity using daily
117 zonal wind data from 2°N–2°S, 140°E–160°E (Figure 3b, see methods).

118 We develop a simple stochastic-trigger El Niño model (STEM) based on
119 extra-tropical and tropical precursor index values in JFMA. The goal is to
120 predict the amplitude of the mature phase of El Niño in December of the same
121 year. In constructing the model, we also incorporate the fact that precursor
122 dynamics translates into stronger El Niño events when the equatorial Pacific

heat content (equivalent to zonal mean thermocline depth) is recharged. We use the mean zonal depth anomaly of the 20 °C isotherm in April across the equatorial Pacific to identify years when the thermocline is charged. This equatorial thermocline index (Figure 3c, ETHI, see methods) has values of 0 when the isotherm is shallower than usual (e.g. discharged state) and values of 1 when the isotherm is deeper than usual (e.g. charged state). We now formalize the STEM model as

$$\text{Niño3(Dec)} = [\alpha \times \text{SLPHI (JFM)} + \beta \times \text{WWBI (JFMA)}] \times [1+ \gamma \times \text{ETHI}] \quad \text{Eq. 1}$$

where α and β are two parameters that represent the relative strength of the North Pacific (SLPHI) and tropical (WWBI) precursors, both normalized to unit variance. In this model the linear prediction based on the SLPHI and WWBI triggers is amplified by the factor $[1+ \gamma \times \text{ETHI}]$, so that when the thermocline is charged the effect of the SLPHI and WWBI triggers is increased by a factor of γ. This factor associated with the ETHI reflects the different linear amplification of ENSO when the triggers act on a favorably pre-conditioned state. However, in this model the preconditioned state alone cannot lead to an El Niño unless the triggers (e.g. SLPHI and WWBI) are active and of the correct sign. By considering the joint effect of the North Pacific and tropical precursors, this model formulation is an extension of previous linear statistical models[26] of ENSO.

145 We test the El Niño model (Eq. 1, STEM) by reconstructing the December
146 values of the Niño3 index from 1958-2013. All available data for SLPHI (JFM),
147 WWBI (JFMA) and ETHI (JFMA) from 1958-2013 (56 samples) are used in a
148 nonlinear least square fitting procedure to estimate the model parameters
149 (α=0.3, β=0.3 and γ=0.8, see methods). The model reconstruction of past Niño3
150 December variability (Figure 3d) is highly correlated with the observed time
151 series (R=0.71, see methods for significance test) and captures the amplitude of
152 the three strongest El Niños in 1972/73, 1982/83 and 1997/98. Using the 2014
153 index values for SLPHI, WWBI, and ETHI we use the model to forecast the
154 December 2014 Niño3 SST anomalies. The model predicts a strong event with
155 an amplitude comparable to that of the 1997/98 El Niño (~3°C).
156 To assess whether this model is robust in forecasting Niño3 amplitudes, we
157 determine the skill of its hindcasts via a cross-validation procedure where a
158 subset of the full 56 annual samples (e.g. 75%, or 42 years) is used to estimate
159 the model parameters and hindcast the remaining independent samples (e.g.
160 25%, or 14 years). This procedure is repeated 200 times using random sets of 42
161 years to predict the remaining 14 years. The resulting ensemble mean hindcast
162 obtained using 75% of the data information (Figure 3e) shows significant skill
163 in reconstructing the Niño3 (R=0.65) (see Figure S1a for errorbars). In
164 particular, the hindcasts identify all three years with temperature anomalies of >
165 2°C, corresponding to strong El Niño events in 1972/73, 1982/83, and 1997/98,
166 and contain no false positives. When performing the hindcasts experiment we
167 also forecast the values for 2014/15, which continue to show amplitudes > 2°C

168 in the ensemble mean. Performing the ensemble mean hindcasts using only 50%
169 of the samples (28/56) to predict the remaining 50% still identifies the same
170 strong events (Figure S1a) with similar overall skill (R=0.64). However, when
171 we use 25% of the samples (14/56) to generate the hindcast, the outlier events
172 are no longer captured (Figure S1a), except for the 2014 forecast. In exploring
173 the sensitivity of the model, we find that as we reduce the number of samples
174 used in estimating the model parameters (e.g. 25% of samples), the nonlinear
175 fitting procedure generates high uncertainty in estimating the amplification
176 parameter γ. This can be understood by considering that as fewer samples are
177 used to construct the model, the chances of missing all three high amplitude El
178 Niños are much higher. The higher amplitude fluctuations are necessary to
179 correctly estimate the amplification. To demonstrate this, we perform the cross-
180 validation analysis by prescribing the amplification factor to its fitted value (γ
181 =0.8). In this case, the hindcasts using 75%, 50% or 25% of data information are
182 robust in estimating the 1972/73, 1982/83, 1997/98 and 2014/15 events as
183 outliers (Figure S1b).

184 To understand why the hindcast model has skill in capturing the outlier El
185 Niño events, we conduct an analysis of the tropical and extra-tropical trigger
186 indices (e.g. WWBI and SLPHI) and their relationship to the thermocline
187 preconditioning (ETHI) (Figure 3a, b and c; Figure S2 for a more detailed
188 view). We find that all the strong El Niño events (e.g. 1972/73, 1982/83,
189 1997/98) occurred when both triggers and the preconditioning are active (e.g.
190 charged state), with at least two of the three factors being stronger than usual

(Figure S2). While the 1972/73 and 1997/98 events share similar characteristics in that the WWB were exceptionally strong and the thermocline subsurface anomalies large, the 1982/83 was dominated by the North Pacific precursor (Figure S2). Based on these results we suggest that when the tropical and extra-tropical triggers coincide, and the equatorial thermocline is charged, the likelihood of an El Niño event peaking by the end of that year is very high. Furthermore, if one or more of the triggers is also particularly strong we find a strong El Niño in the observed record (Figure S2), with the obvious caveat of very small sample size. To the extent that this finding is robust, the anomalously strong activity of both North Pacific and tropical precursors in 2014 JFMA leads to STEM prediction for the development of a strong El Niño in the winter of 2014/15 (Figure 3).

The stochastic-trigger El Niño model (Eq. 1, STEM) presented in this study combines key mechanisms of tropical and extratropical stochastic forcing of El Niño, which when aligned appear to lead to the development of strong El Niño events. The assumptions underlying this model imply that El Niño events can be interpreted as a "series of events" (ref. 5) rather than a damped oscillation – that is there is no memory needed between events. Moreover, strong events are outliers only because they are triggered by unusually large initial noise events. To verify if this view is consistent with observations we explore the statistics of El Niño occurrence rate using a 50,000-year simulation of STEM. The simulation is executed by repeatedly generating 56-year-long random samples (with replacement) from the observed distribution of SLPHI, WWBI and ETHI

so that no correlation exists between the predictor indices. The resulting model statistics recover the observed occurrence rate of El Niño events within errorbars (Figure 4), suggesting that the stochastic paradigm (e.g., refs. 7,27,28) is a valid null-hypothesis for ENSO dynamics.

The model prediction of a strong 2014/15 event (Figure 3e) presents a clear test of the stochastic-trigger framework for ENSO dynamics. Still there are several physical factors that this model does not include. For example, this model does not account for the precise timing of the triggers (e.g. WWB) in the spring preceding an El Niño, which may play a key role determining the amplitude of a strong El Niño. Furthermore, the STEM does not account for mean state dependencies, which may play an important role in the growing stages of El Niño events[29]. Dynamical forecast models of ENSO currently (April, 2014) predict a weak to moderate El Niño event for the winter of 2014/15 with a likelihood of over 65% (ref. 30). However, if our stochastic-trigger El Niño model prediction turns out to be correct, a reassessment of the representation of tropical and extratropical triggers in climate models may be warranted.

METHODS

We use monthly SLPa and daily zonal winds from the National Centers for Environmental Prediction/National Center for Atmospheric Research (NCEP/NCAR) Reanalysis Project[31] and SSTa from the National Oceanic and Atmospheric Administration (NOAA) Extended Reconstruction sea surface temperatures (NOAA ERv3; ref. 32) from January 1950 to April 2014. The thermocline temperature data of Figure 1 comes from the NCEP Global Ocean Data Assimilation (GODAS; ref. 33). Monthly anomalies are computed for each data set by removing the climatological monthly means.

To extract the modes of co-variability of the ocean and atmosphere in the Pacific Ocean (Figure 2), we use simultaneous Empirical Orthogonal Functions (EOFs) of the SLPa and SSTa fields, referred to here as SEOF. In SEOFs, two or more data fields are put into one large space and time matrix that is subsequently decomposed via singular value decomposition. Prior to computing the SEOFs, the SSTa is normalized by the domain average standard deviation and the SLPa normalized along each latitude by the standard deviation at that latitude. The data are smoothed in time using a 4-month running mean.

The westerly wind burst index (WWBI) in Figure 3 is computed using the daily zonal wind in the box (2°S–2°N, 140°E–160°E). We take a cumulative sum of all positive occurrences in the months of JFMA from 1950–2014 to generate the WWBI (JFMA). The cumulative sum measures the integrated effect of westerly wind bursts on the equatorial thermocline.

The equatorial thermocline index (ETHI) is computed using the European Centre for Medium-Range Weather Forecasts (ECMWF) Ocean Reanalysis System 4 (ORA-S4; ref. 34). We take the zonal mean of the isotherm 20°C depth anomaly in the month

of April. When the zonal mean is larger or equal to zero we label the index as charged (ETHI = 1), when negative we label as neutral or discharged (ETHI = 0). Because the ORA-S4 data for April 2014 was not available we used the GODAS dataset to determine that the thermocline was charged in 2014 (ETHI = 1).

The North Pacific SLPa index over Hawaii (SLPHI) is computed by averaging the JFM SLPa over the box in Figure 2a (10°N–20°N, 160°W–140°W).

To compute the STEM model parameters (Eq. 1) we used a nonlinear least square fitting procedure in MATLAB (lsqcurvefit.m) that minimizes the sum of the squared differences between the data and model prediction. The optimal parameter set is α=0.3, β=0.3, and γ=0.8. A sensitivity of the model reconstruction skill to the number of model parameters (Figure S3) shows that inclusion of all parameters improves the model skill and eliminates false positives in the reconstruction. Cross validation is done in the following manner: one quarter of the data is withheld to serve as "independent" data for hindcast purposes; years are chosen randomly. The remaining "training" data is then centered (i.e., adjusted to have zero mean) and standardized to have unit standard deviation; the parameters α, β, and γ are then determined for this subsample. The independent data are then centered about the training data sample means and are normalized by the training data sample standard deviation, and finally hindcasts for this period are made using the parameters from the training data. This procedure is repeated 200 times; the ensemble mean skill of the hindcasts is displayed in Figure 3.

The significance of the correlation coefficients is estimated from the Probability Distribution Functions (PDFs) of the correlation coefficient of two red-noise time series with the same auto regression coefficients as estimated from the original signals. The PDFs are computed numerically by generating 3000 realizations of the correlation coefficient of two random red-noise time series.

References

1 Su, H., Neelin, J. D. & Chou, C. Tropical teleconnection and local response to SST anomalies during the 1997–1998 El Niño. *J. Geophys. Res. Atmospheres* **106**, 20025–20043, doi:10.1029/2000jd000124 (2001).

2 Messie, M. & Chavez, F. P. A global analysis of ENSO synchrony: The oceans' biological response to physical forcing. *J. Geophys. Res. Atmospheres* **117**, doi:10.1029/2012jc007938 (2012).

3 Widlansky, M. J., Timmermann, A., McGregor, S., Stuecker, M. F. & Cai, W. An interhemispheric tropical sea level seesaw due to El Niño Taimasa. *J. Climate* **27**, 1070–1081, doi:10.1175/JCLI-D-13-00276.1 (2014).

4 Jin, F.-F. An equatorial ocean recharge paradigm for ENSO. Part I: Conceptual model. *J. Atmos. Sci.* **54**, 811–829 (1997).

5 Kessler, W. S. Is ENSO a cycle or a series of events? *Geophys. Res. Lett.* **29**, doi:10.1029/2002gl015924 (2002).

6 Fedorov, A. V. The response of the coupled tropical ocean-atmosphere to westerly wind bursts. *Quart. J. Roy. Meteor. Soc.* **128**, 1–23 (2002).

7 Penland C. & Sardeshmukh, P. D. The optimal growth of tropical sea surface temperature anomalies. *J. Climate* **8**, 1999–2024 (1995).

8 Vimont, D., Battisti, D. & Hirst, A. Footprinting: A seasonal connection between the tropics and mid-latitudes. *Geophys. Res. Lett.* **28**, 3923–3926 (2001).

9 Anderson, B. T. Tropical Pacific sea-surface temperatures and preceding sea level pressure anomalies in the subtropical North Pacific. *J. Geophys. Res. Atmospheres* **108** (2003).

10 Tollefson, J. El Niño tests forecasters. *Nature* **508**, 20–21 (2014).

11 Moore A. M. & Kleeman, R. The dynamics of error growth and predictability in a coupled model of ENSO. *Quart. J. Roy. Meteor. Soc.* **122**, 1405–1446 (1996).

12 Kleeman R. & Moore, A. M. A theory for the limitation of ENSO predictability due to stochastic atmospheric transients. *J. Atmos. Sci.* **54**, 753–767 (1997).

13 Moore, A. M. & Kleeman, R. Stochastic forcing of ENSO by the intraseasonal oscillation. *J. Climate* **12**, 1199–1220, doi:10.1175/1520-0442 (1999).

14 McPhaden, M. J. Genesis and evolution of the 1997–98 El Niño. *Science* **283**, 950–954 (1999).

15 McPhaden, M. J. & X. Yu. Equatorial waves and the 1997–98 El Niño. *Geophys. Res. Lett.* **26**, 2961–2964 (1999).

16 Kessler W. S. & Kleeman, R. Rectification of the Madden-Julian Oscillation into the ENSO cycle. *J. Climate* **13**, 3560–3575 (2000).

17 Chang P. *et al.* Pacific meridional mode and El Niño/Southern Oscillation. *Geophys. Res. Lett.* **34**, doi:10.1029/2007GL030302 (2007).

18 Alexander, M. A., L. Matrosova, C. Penland, J. D. Scott & Chang, P. Forecasting Pacific SSTs: Linear inverse model predictions of the PDO. *J. Climate* **21**, 385–402 (2008).

19 Alexander, M. A. in *Climate Dynamics: Why does Climate Vary* Vol. 189 (eds D. Sun & F. Bryan) 123–148 (AGU Monograph, Washington D. C., 2010).

20 Newman, M., M. A. Alexander & Scott, J. D. An empirical model of tropical ocean dynamics. *Climate Dyn.*, doi:10.1007/s00382-011-1034-0 (2011).

21 H. Freeland & Whitney, F. Vol. 22 (ed PICES Press) (2014).

22 Chiang, J. C. H. & Vimont, D. J. Analagous meridional modes of atmosphere-ocean variability in the tropical Pacific and tropical Atlantic. *J. Climate* **17**, 4143–4158 (2004).

23 Xie, S.-P. A dynamic ocean-atmosphere model of the tropical Atlantic decadal variability. *J. Climate* **12**, 64–70 (1999).
24 Knutson, T. R. & Manabe, S. Model assessment of decadal variability and trends in the tropical Pacific Ocean. *J. Climate* **11**, 2273–2296, doi:10.1175/1520-0442 (1998).
25 Anderson B. T., J. C. Furtado, K. M. Cobb & Di Lorenzo, E. Extratropical forcing of El Niño–Southern Oscillation asymmetry. *Geophys. Res. Lett.* **40**, 4916–4921, doi:10.1002/grl.50951 (2013).
26 McPhaden, M. J., X. B. Zhang, H. H. Hendon & Wheeler, M. C. Large scale dynamics and MJO forcing of ENSO variability. *Geophys. Res. Lett.* **33**, doi:10.1029/2006gl026786 (2006).
27 Moore, A. M. & Kleeman, R. The singular vectors of a coupled ocean-atmosphere model of ENSO. 1. Thermodynamics, energetics and error growth. *Quart. J. Roy. Meteor. Soc.* **123**, 953–981 (1997).
28 Moore, A. M. & Kleeman, R. The singular vectors of a coupled ocean-atmosphere model of ENSO. 2. Sensitivity studies and dynamical interpretation. *Quart. J. Roy. Meteor. Soc.* **123**, 983–1006 (1997).
29 Fedorov, A. V. & Philander, S. G. H. A stability analysis of tropical ocean-atmosphere interactions: Bridging measurements and theory for El Niño. *J. Climate* **14**, 3086–3101 (2001).
30 Becker, E. *May 8 ENSO Diagnostic Discussion*, <http://www.climate.gov/news-features/blogs/enso/may-8-enso-diagnostic-discussion> (2014).
31 Kanamitsu, M. *et al.* NCEP-DOE AMIP-II Reanalysis (R-2). *Bull. Amer. Meteor. Soc.* **83**, 1631–1643 (2002).
32 Smith, T. M., Reynolds, R. W., Peterson, T. C. & Lawrimore, J. Improvements to NOAA's historical merged land-ocean surface temperature analysis (1880-2006). *J. Climate* **21**, 2283-2296, doi:10.1175/2007JCLI2100.1 (2008).
33 Behringer, D. W. & Xue, Y. in *Eighth Symposium on Integrated Observing and Assimilation Systems for Atmosphere, Oceans, and Land Surface, AMS 84th Annual Meeting* (Seattle, Washington, 2004).
34 Balmaseda, M. A., Mogensen, K. & Weaver, A. T. Evaluation of the ECMWF ocean reanalysis system ORAS4. *Quart. J. Roy. Meteor. Soc.* **139**, 1132–1161, doi:10.1002/qj.2063 (2013).

Acknowledgements

We acknowledge the support of the NSF OCE-0550266, GLOBEC-0606575, OCE-0452654, OCE-0452692, CCS-LTER, GLOBEC OCE-0815280, OCE05-50233, NASA NNG05GC98G, Office of Science (BER), NOAA-MAPP, DOE DE-FG02-07ER64469 and JAMSTEC.

Author Contributions

EDL, MN, AT and BA performed the statistical analysis. EDL, KC, MN, NS, BA, AT and MJW contributed to the writing of the paper. AT and MN contributed the model cross-validation analyses. HF provided observational analysis for the North Pacific. All authors discussed and commented on the layout and the results of the manuscript.

FIGURE LEGENDS

1. **Figure 1 | Tropical and extra-tropical precursors of El Niño. a**, Regression of December Niño3 index with GODAS equatorial temperatures in April and WWB index derived from the NCEP zonal wind anomalies in JFMA between 2°S–2°N, 140°E–160°E (orange arrow, see methods for index definition). WWB index is in units of standard deviations. **b**, Regression of December Niño3 index with North Pacific SSTa in JFMA. **c, e, g** April thermocline with the WWB anomalies in JFMA (orange arrows) for the years 1982, 1997 and 2014. **d, f, h** JFM North Pacific SSTa for the years 1982, 1997 and 2014.

2. **Figure 2 | The 2nd mode of ocean-atmosphere co-variability of the Pacific. a**, Correlation of the mode in the SLPa. **b**, Regression of the mode with SSTa **c**, Temporal evolution of the principal component (blue line) leading the principal component of the 1st mode (ENSO) by 12 months. The correlation of 0.62 is significant (see methods).

3. **Figure 3 | The stochastic-trigger El Niño model forecast. a**, Timeseries of the North Pacific El Niño precursor (SLPHI, blue line) in JFM. **b**, Timeseries of the tropical El Niño precursor (WWBI, orange line) in JFMA. **c**, Timeseries of the equatorial thermocline charge index (ETHI, green line). **d**, Comparison of model reconstruction (black line) with the Niño3 Index (red line). **e**, Comparison of model ensemble forecast with Niño3 Index. The

406 forecasts ensemble was generated using random sets of 75% of the data to
407 forecast the remaining 25%.

408 4. **Figure 4 | Statistics of El Niño occurrence rate over a 56 year period.** The
409 y-axis is the percentage of events with a temperature higher than indicated by
410 the respective x-axis value. (red dots) Observed December Niño3 index
411 values. (black line) Statistics of the stochastic-trigger El Niño model (STEM)
412 from a 50,000 year simulation, ±1 standard deviation (STD) (gray lines). The
413 STEM model simulation is executed by randomly sampling the distribution of
414 SLPHI, WWBI and ETHI so that no correlation exists between the predictor
415 indices. The sampling is done so that on a 56 year period the same values of
416 any index can be selected more than once.

417 5. **Supplemental Figure 1 | Forecast Model sensitivity. a,** Ensemble mean
418 forecasts (black lines) using partial sets of information (e.g. 75%, 50% and
419 25%) to estimate the model parameters. Error bars are in black brackets. The
420 red curve is the Niño3 index in December. **b**, Same as panel **a** but with a
421 fixed amplification factor set to its optimal value (γ=0.8).

422 6. **Supplemental Figure 2 | Precursor conditions prior to El Niños. a**,
423 Timeseries of North Pacific Precursor SLPHI in JFM. **b**, Timeseries of
424 tropical precursor WWBI in JFMA. **c**, Timeseries of zonal mean isotherm 20
425 °C anomaly in April. **d**, Hovmueller diagram of isotherm 20 °C anomaly
426 along the equator.

7. **Supplemental Figure 3 | Sensitivity of STEM model to number of parameters.** Top panels compare the model reconstruction (black line) using the set of parameters indicated above the frame with the Niño3 December values (red line). The significance test for the correlation is reported in the bottom panels with the probability distribution function from the Montecarlo test (see methods).

8.

Figure 1

Tropical and Extra-tropical El Niño Precursors

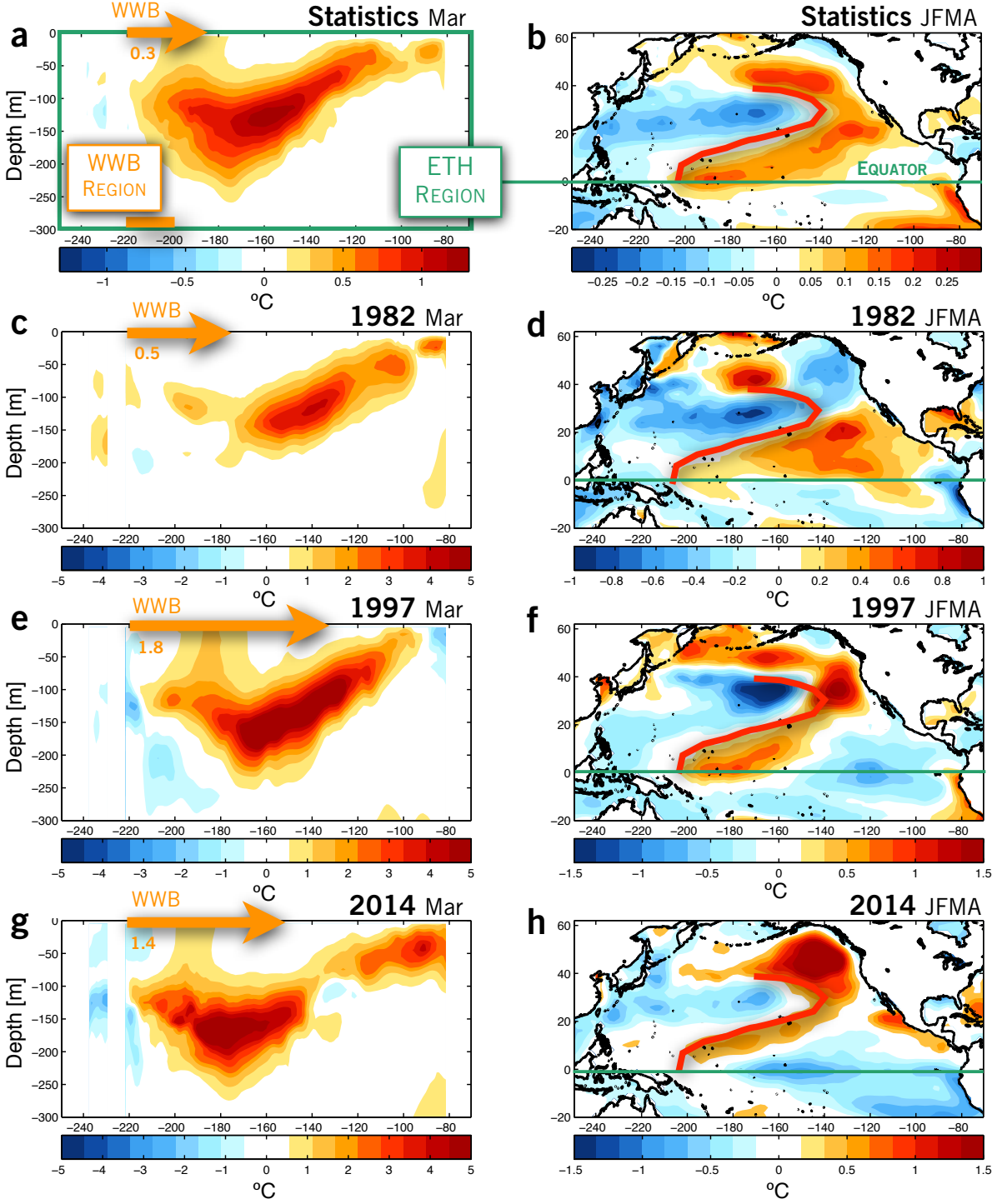

Figure 2

The North Pacific El Niño Precursor

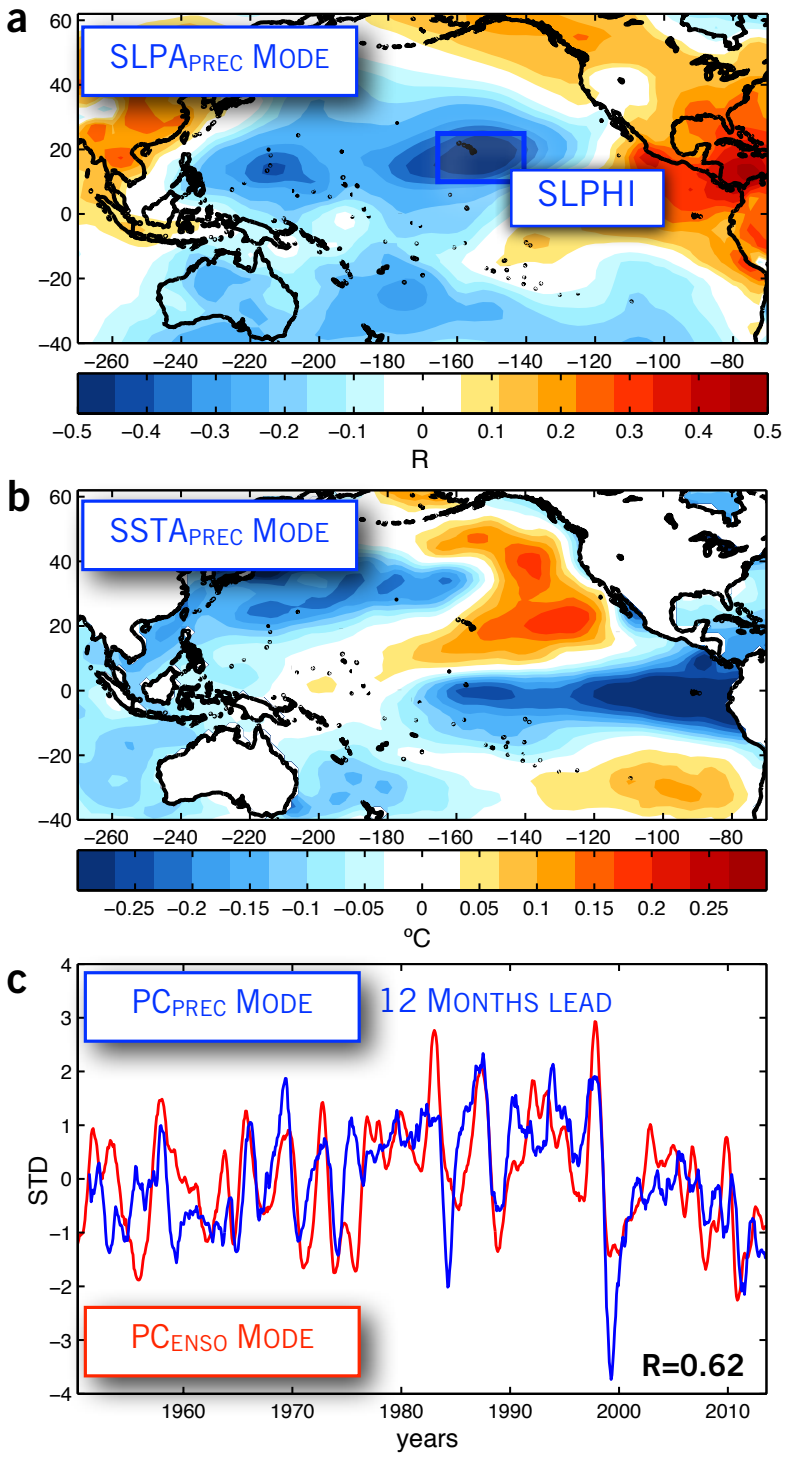

Figure 3

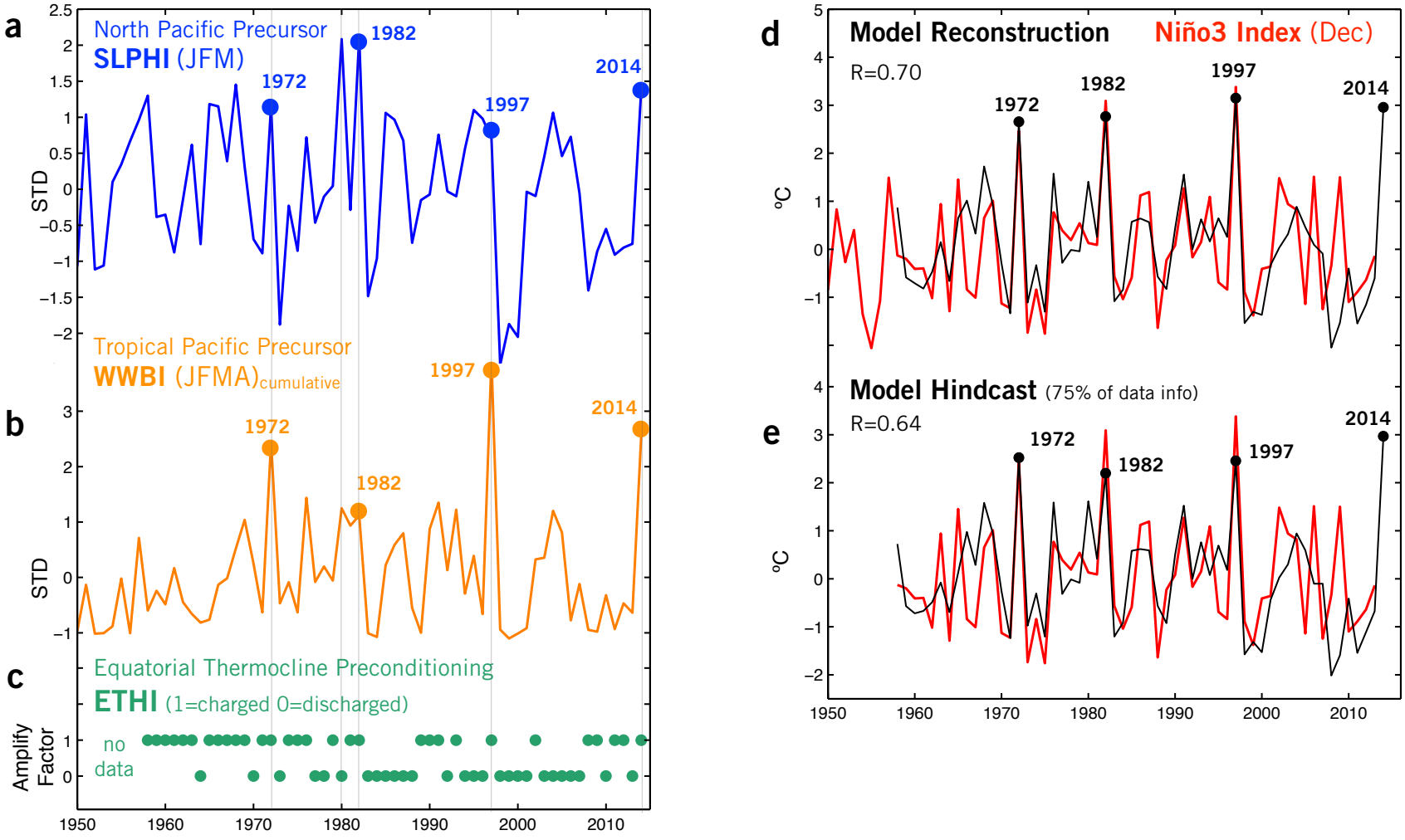
a
North Pacific Precursor
SLPHI (JFM)
1972
1982
1997
2014
STD
b
Tropical Pacific Precursor
WWBI (JFMA)cumulative
1972
1982
1997
2014
STD
c
Equatorial Thermocline Preconditioning
ETHI (1=charged 0=discharged)
no data
Amplify Factor
1950
1960
1970
1980
1990
2000
2010
d
Model Reconstruction
Niño3 Index (Dec)
R=0.70
1972
1982
1997
2014
°C
e
Model Hindcast (75% of data info)
R=0.64
1972
1982
1997
2014
°C

Figure 4

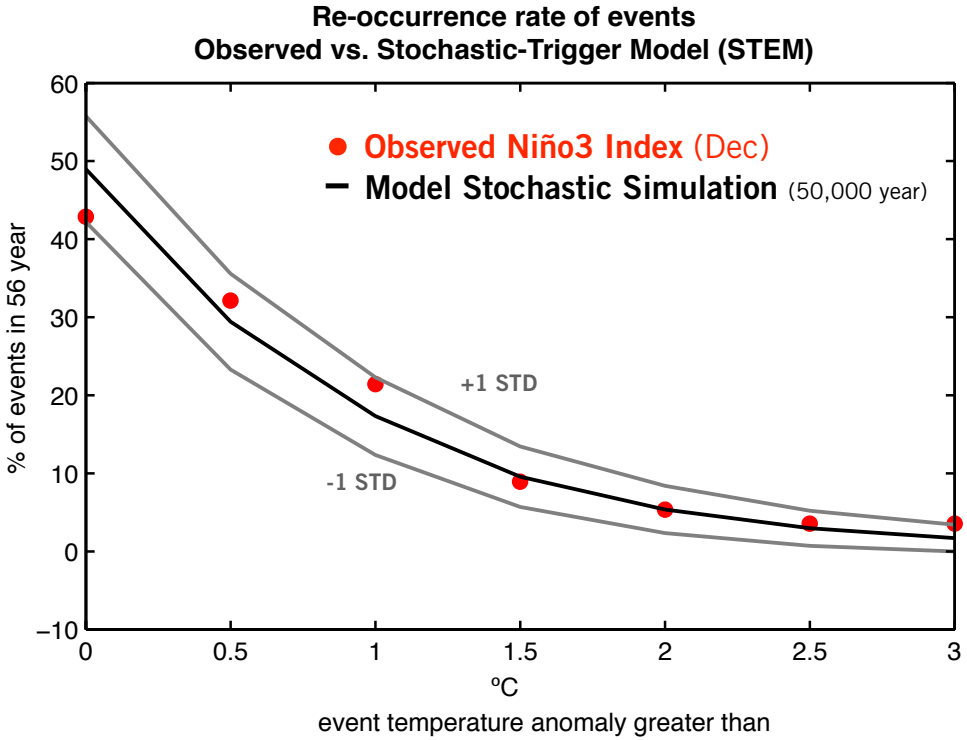
Re-occurrence rate of events
Observed vs. Stochastic-Trigger Model (STEM)
Observed Niño3 Index (Dec)
Model Stochastic Simulation (50,000 year)
+1 STD
-1 STD
% of events in 56 year
60
50
40
30
20
10
0
−10
0
0.5
1
1.5
2
2.5
3
°C
event temperature anomaly greater than

Supplemental Figure 1 **STEM model sensitivity**

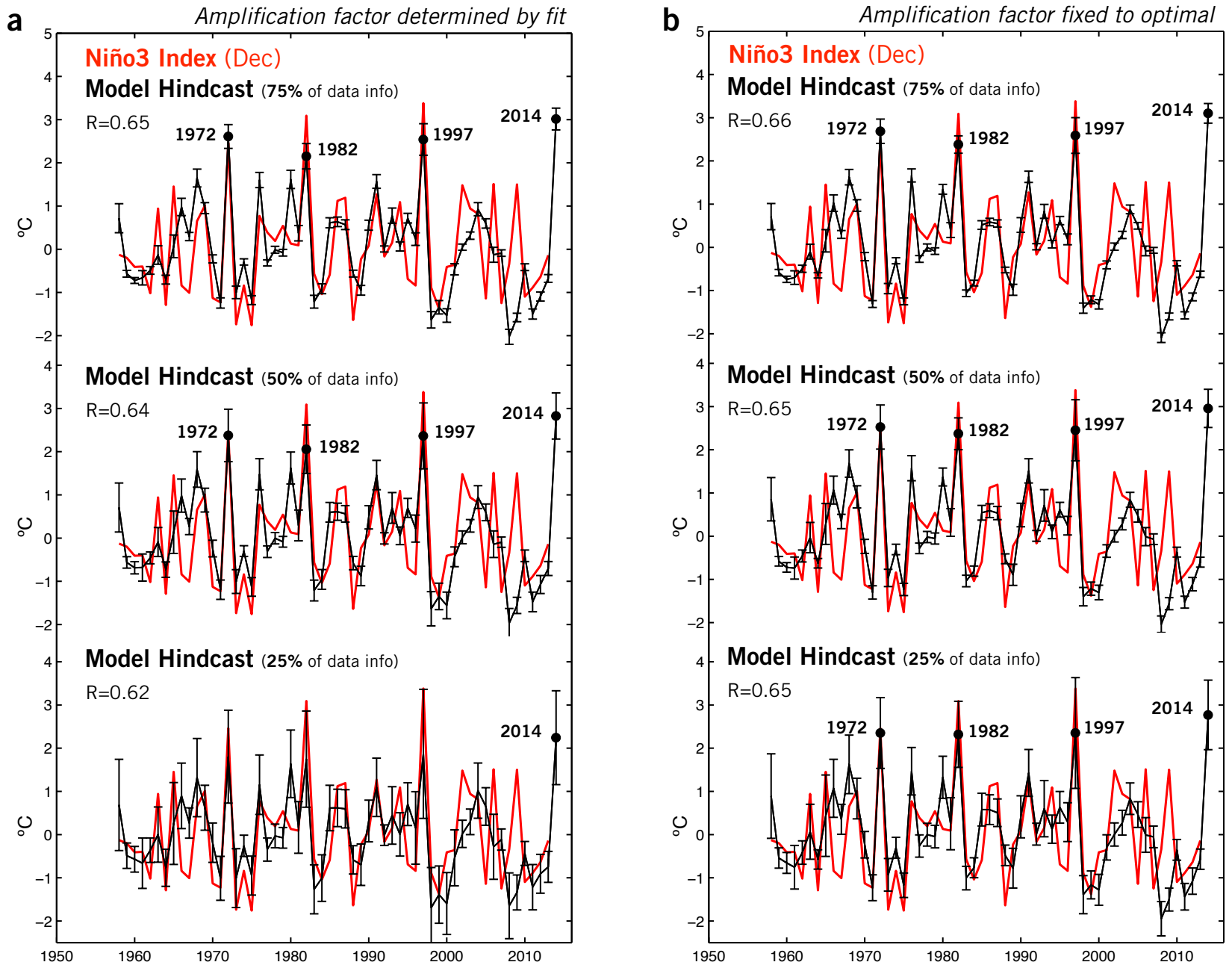

Supplemental Figure 2

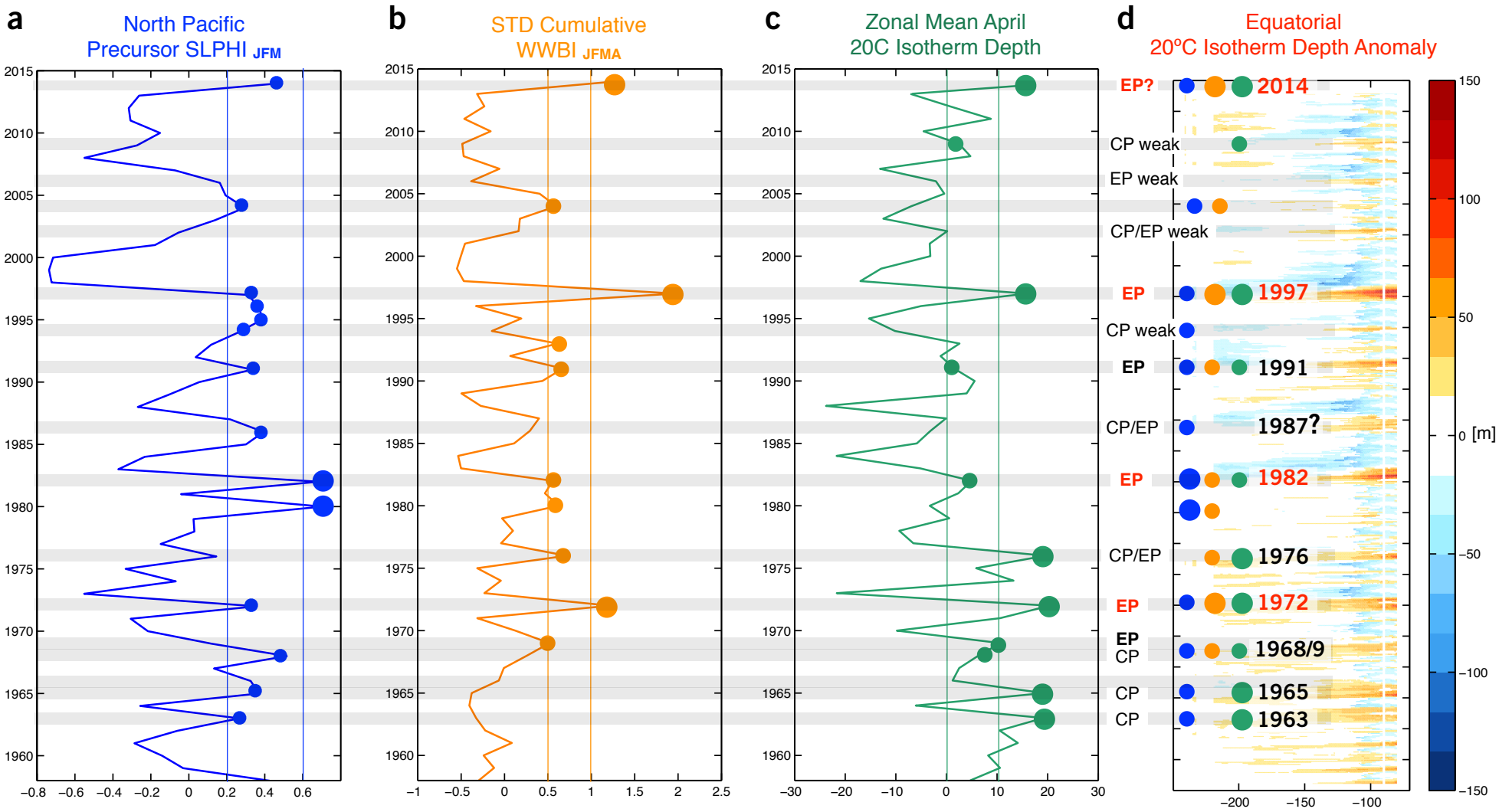

Supplemental Figure 3